Available online at www.sciencedirect.com
SCIENCE DIRECT®
Tectonophysics 361 (2003) 121–137
TECTONOPHYSICS
www.elsevier.com/locate/tecto

Numerical modeling of strike-slip creeping faults and implications for the Hayward fault, California

R. Malservisi*, C. Gans, K.P. Furlong

Geodynamics Research Group, Department of Geosciences, Pennsylvania State University, 542 Deike Building, University Park, PA 16801, USA

Received 24 September 2001; accepted 11 October 2002

Abstract

The seismic potential of creeping faults such as the Hayward fault (San Francisco Bay Area, CA) depends on the rate at which moment (slip deficit) accumulates on the fault plane. Thus, it is important to evaluate how the creep rate observed at the surface is related to the slip on the fault plane. The surface creep rate (SCR) depends on the geometry of locked and free portions of the fault and on the interaction between the fault zone and the surrounding lithosphere. Using a viscoelastic finite element model, we investigate how fault zone geometries and physical characteristics such as frictionless or locked patches affect the observed surface creep when the system is driven by far field plate motions. These results have been applied to creep observations of the Hayward fault. This analysis differs from most previous fault creeping models in that the fault in our model is loaded by a distributed viscous flow induced by far field velocity boundary conditions instead of imposed slip beneath the major faults of the region. The far field velocity boundary conditions simulate the relative motion of the stable Pacific plate respect to the Rigid Sierra Nevada block, leaving the rheology, fault geometry, and mechanics (locked or free to creep patches), to determinate the patterns of fault creep.

Our model results show that the fault geometry (e.g. length and depth of creeping) and the local rheology influence the surface creep rate (SCR) and the slip on the fault plane. In particular, we show that the viscoelastic layer beneath the elastic seismogenic zone plays a fundamental role in loading the fault. Additionally, the coupling with the surrounding lithosphere results in a smooth transition from regions free to creep to locked patches.

Keywords: Creeping faults; Hayward fault; Numerical modeling; Lithospheric dynamics; Lithospheric rheology

1. Introduction

Strike-slip faults, while mostly remaining locked between large stress-releasing events, can, in some cases, creep. Surface creep has been documented in two major continental strike-slip fault systems: the North Anatolian fault in Turkey (e.g. Ambraseys, 1970; Aytun, 1980; Sylvester, 1988) and the San Andreas and its related faults in California (e.g. Lienkaemper et al., 1991; Galehouse, 1992; Lienkaemper and Galehouse, 1998). Although the occurrence of creep is documented, the interactions between locked and creeping portions of a fault and

* Corresponding author. Present address: RSMAS-MGG University of Miami, 4600 Rickenbacker Causeway, Miami, FL 33149, USA. Tel.: +1-305-361-4928; fax: +1-305-361-4632.
E-mail address: rmalservisi@rsmas.miami.edu. (R. Malservisi).

0040-1951/02/$ - see front matter © 2002 Elsevier Science B.V. All rights reserved.
PII: S0040-1951(02)00587-5

the conditions that lead to creep are not well understood.

Fault creep is an important issue, especially for earthquake risk assessment. The causes and the depth extent of creep on faults are not typically known, making risk assessment problematic. If creep extends through the seismogenic layer and matches the long-term slip rates, then earthquakes would not likely initiate on that area of the fault. However, if the creeping zone extends only to a shallow depth, or if the creep velocity does not match the long-term slip rate, a slip deficit can build, increasing the potential seismic moment for an earthquake on that segment of the fault.

The geometry of the fault section able to creep (unlocked), the length of the creeping section, the degree of coupling with the surrounding lithosphere, and the rheological properties of the lithosphere all play fundamental roles in the creeping process. Previous analyses reached conflicting conclusions as to the extent of creep on the Hayward fault. Prescott and Lisowski (1985) suggest deep slip on the fault based on limited comparison of near field and far field geodetic data. Lienkaemper et al. (1991) could not resolve patterns of slip on the Hayward fault. Savage and Lisowski (1993), Bürgmann et al. (2000), Simpson (2000), and Simpson et al. (2001) all have proposed differing models for the extent and depth of creep on the Hayward fault. Using a 2-D model, Savage and Lisowski (1993) proposed that the creeping zone on the Hayward fault extends to ~5 km depth, with the fault locked from 5 km to the base of the seismogenic layer. Bürgmann et al. (2000) suggest little, if any, locking along the northern Hayward fault. They inverted the surface creep rate (SCR) and the local long-term strain field to estimate the amount of creep on the fault plane and to map the area with a slip deficit. Bürgmann et al. (2000) used GPS and InSAR data to constrain a dislocation model where slip rates are formally inverted from the data

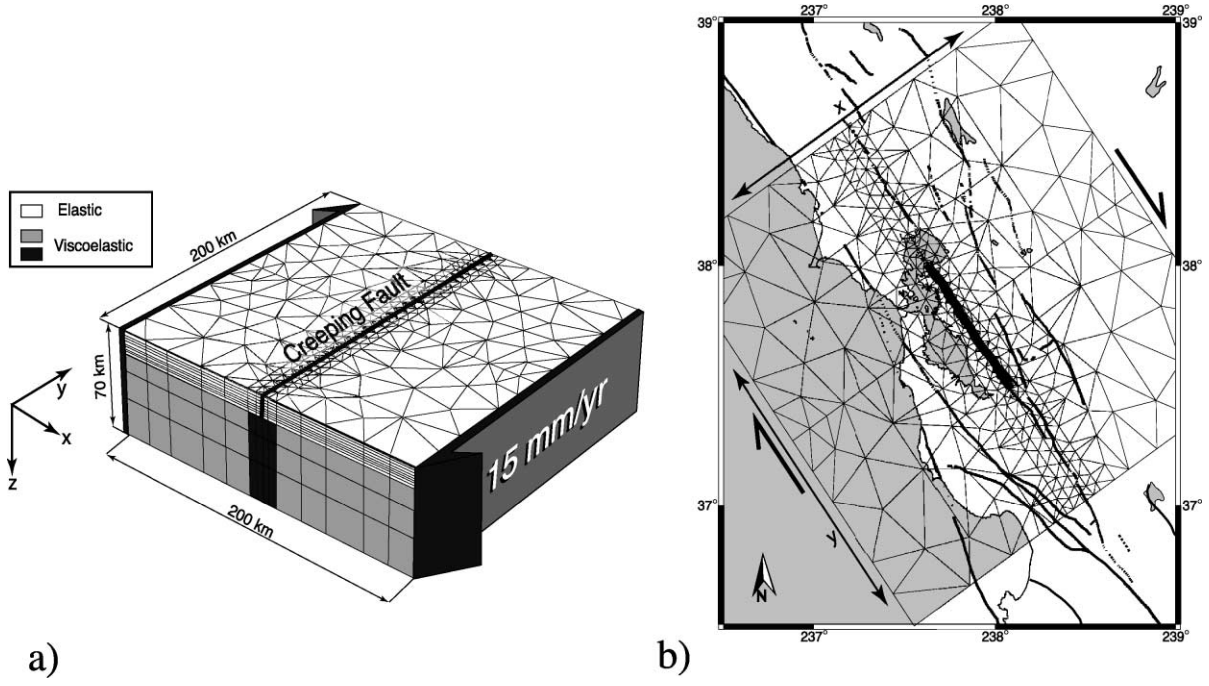

Fig. 1. (a) Geometry and mesh for the finite element modeling in this study. The lithosphere is simulated through a 12-km-thick elastic layer (white) over a linear viscoelastic region (gray). The dark gray region is assigned the same viscosity of the light gray area (homogeneous models) or a lower viscosity (shear zone models). A far field velocity boundary condition drives the system. The dark line at the center of the model represents the fault and specifies the area that can be allowed to creep. (b) Extent of the model in the geographic reference of the San Francisco Bay area. The thick lines indicate the active faults mapped in the area (Jennings, 1994). The thickest line at the center of the mesh indicates the creeping segment of the Hayward fault.

while varying locking depth on the main fault in the region. They used those results and 3-D boundary element model driven by deep dislocation to evaluate the fault creep rate. They argue that previous geodetic data did not allow for creep depth differentiation, but the addition of the GPS and InSAR data mitigates that problem. A best-fit to the geodetic and InSAR data is obtained when the northern 20 km of the Hayward fault is allowed to creep throughout the seismogenic zone, and creep in the south is restricted to shallower depths. Simpson et al. (2001), on the other hand, matched surface creep rate data using a different 3-D boundary element model formulation, obtaining a significantly different pattern of fault creep.

A recently implemented approach for modeling fault/lithosphere interaction (Malservisi et al., 2001) allows us to address fault creep in a different way and to test the influence of tectonic forces on the creeping process. In particular, we can test the response of fault segments to the far field velocities and evaluate what conditions promote fault zone creep.

The Hayward fault (Fig. 1) located on the east side of San Francisco Bay is part of the San Andreas fault system and is a well-documented creeping fault. At the surface, it is undergoing right-lateral creep at an average rate of 5 mm/year, as compared to an inferred long-term fault slip rate of 9–10 mm/year (Lienkaemper et al., 1991, 2001; Galehouse, 1992; Lienkaemper and Galehouse, 1998; Bürgmann et al., 2000). The last major earthquake on the 82-km-long fault ($M = \sim 6.8$) occurred in 1868, with surface rupture over the southern ~ 60 km of the fault (Lienkaemper et al., 1999). Prior to the 1868 event, there is evidence for another earthquake on the northern segment of the Hayward fault between 1640 and 1776 AD (Toppozada and Borchart, 1998; Lienkaemper et al., 1999).

In all of the previous models (i.e. Savage and Lisowski, 1993; Bürgmann et al., 2000; Simpson et al., 2001), the goal was to fit surface geodetic data by specifying patterns of creep on the fault. In our modeling, we impose a far field relative velocity on the sides of the model (Fig. 1a) to examine the conditions under which creep can occur. Our models allow for "creepable" elements that have the potential to creep, but are not forced to do so. This approach allows us to test the influence of various parameters (e.g. fault length, viscosity, and geometry of the creepable/locked zones) on the potential of a fault to undergo creep.

2. The model

Our model approach allows us to test the conditions that drive creep on a fault in response to velocity boundary conditions applied in the far field. The goal is to examine the relationship between the physical characteristics of a fault and its potential to creep. We use a 3-D version of the finite element code TECTON (Melosh and Raefsky, 1980; Govers, 1993; Govers et al., 2000; Govers and Meijer, 2001) to simulate different crust/lithosphere rheologies, fault geometries, and fault properties (free/locked patches). Fig. 1 shows the model geometry and the geographic position of the mesh. The model is 200 km wide (x direction, $\sim$ SW–NE), 200 km long (y direction, $\sim$ NW–SE), and 70 km thick (z direction). We simulate the lithosphere as a two-layer block. A shallow elastic layer represents the seismogenic crust, overlays a viscoelastic layer with a Maxwell (linear) rheology and variable viscosities that simulate the lower crust/upper mantle. Consistent with the thickness of the seismogenic layer along the Hayward fault, we specify the elastic layer to be 12 km thick. Microseismicity studies in the Hayward region show that the seismogenic layer is confined to the top 12 km (Waldhauser and Ellsworth, 2000). We have tested the effect of viscosity variations in the viscoelastic layer and of a lower viscosity area localized beneath the creeping fault on creep behavior (viscosity ranging from 10^{18} to 10^{21} Pa·s). The low viscosity region is included to simulate the presence of a narrow shear zone associated with the evolution of the North America/Pacific plate boundary due to the migration of the Mendocino Triple Junction (Furlong et al., 1989; Furlong, 1993; Furlong and Verdonck, 1993). In both the layers, we assume a Young's module of 50 GPa and a Poisson ratio of 0.3.

The creeping fault is defined using the method of "slippery nodes" (Melosh and Williams, 1989). By adding a degree of freedom to a specific node, the method allows the slippery node to behave as if it were split into two parts. This allows a differential displacement along a fixed direction without friction. The actual amount of differential displacement depends

on the local force field. In this way, the slippery nodes represent the areas of the fault plane that have the potential to creep. In the models presented here, the fault plane is defined as a vertical plane oriented in the y direction, passing through the center of the model ($x=0$). The fault is symmetric with respect to the center of the mesh (tips at $y=L/2$, where $L=$ length of the fault) and free to creep from the surface to a specified depth in the seismogenic layer (maximum depth = 12 km). All the slippery nodes on this plane can potentially creep along the fault plane direction ("creepable" nodes) and the amount of differential displacement is dependent on the local force field. To define locked patches on the fault plane, we specify the corresponding nodes as "bound" or not slippery.

In all the models, the creep rate is defined as the average of differential displacement across the fault plane at two times steps divided by the time. In this way, creep is zero on all locked sections and within the viscoelastic layer, although elastic or viscoelastic deformation may occur in those regions.

In the San Francisco Bay area, the Pacific plate moves at ~ 47 mm/year with respect to the North America plate (DeMets et al., 1994). Approximately 12 mm/year of this plate motion is accommodated along the Eastern California shear zone (e.g. Dixon et al., 2000) leaving about 35 mm/year to be accommodated in the San Francisco Bay area (comparable with regional GPS and InSAR observations, e.g. Bürgmann et al., 2000; Argus and Gordon, 2001). Furlong et al. (1989) suggested that deep creep on the San Andreas alters the velocity field and Lisowski et al. (1991) indicated that that creep produces ~ 5 mm/year near the San Andreas fault. The single fault model that we utilize in this study assumes that the remaining relative displacement is the far field velocity that drives the creeping on the Hayward fault. Thus, a far field relative velocity of 30 mm/year drives the deformation of our models. This is implemented as an applied velocity boundary condition along the side of the mesh (± 15 mm/year at $x=\pm 100$ km, Fig. 1) in a direction parallel to the fault. In order to minimize the effect of the singularity at the tip of the fault and since the models do not include gravitational nor isostatic forces, no vertical displacement is allowed at the top and bottom surfaces ($z=0$ and 70 km, respectively).

3. General parameters influencing creeping behavior

We ran a suite of models to test the influence of different fault parameters on creeping behavior. Table 1 lists the parameters used in all our models, with a short definition of each. The first set of model runs was intended to test effects of rheological properties. Models 1–3 are described in Table 2. Once the best rheological model was determined, different model geometries were studied. Models 4–6 are described in Table 3.

3.1. Fault length

The length of the "creepable" section of the fault is one of the main controls on the maximum surface creep rate (MSCR). This result is compatible with the observed relationship between fault length and geological slip rate (i.e. Bilham and Bodin, 1992). Fig. 2 summarizes the variation of MSCR as a function of fault length for different rheological models. In this set of simulations, the fault cuts through the entire seismogenic layer (0–12 km) and is "creepable" from $y=-L/2$ to $y=L/2$. The infinite fault case is simulated by defining all the

Table 1
Parameters

Parameter	Description	Range/value
L	Length: fault length	10 km–∞
MSCR	Maximum Surface Creep Rate: maximum creeping rate at the surface along the fault plane	mm/year
SCR	Surface Creep Rate: creeping rate at the surface along the fault plane as a function of position	mm/year
TLD	Top Locking Depth: depth at which the creeping section of the fault connected to the surface is locked	0–12 km
BLD	Bottom Locking Depth: depth below which the seismogenic layer is allowed to creep	0–12 km

Table 2
Rheological models

Model name	Viscosity viscoelastic layer (Pa·s)	Viscosity low viscosity zone (Pa·s)	Viscoelastic layer
Model 1a	1×10^{18}	1×10^{18}	homogeneous
Model 1b	1×10^{19}	1×10^{19}	homogeneous
Model 1c	1×10^{21}	1×10^{21}	homogeneous
Model 2	1×10^{20}	1×10^{18}	with shear zone
Model 3	1×10^{21}	1×10^{18}	with shear zone

nodes of the elastic layer on the plane $x=0$ km as slippery. The MSCR increases as the fault becomes longer and asymptotically approaches the value for an infinite length fault (horizontal line in the graph). For each modeled rheology, the relationship between MSCR and the length of the creeping section of the fault seem to follow an exponential expression of the form

$$(\mathrm{MSCR}) = -A\mathrm{e}^{-\frac{L}{B}} + C$$

where A and B are model-dependent constants, and C is the asymptotic (infinite fault length) value (dashed line in Fig. 2) and it is related to the loading strain rate in the viscoelastic layer beneath the fault.

3.2. Lower lithosphere viscosity

In the case of homogeneous viscosity, the MSCR is not sensitive to the absolute value of the viscosity. Results for an 80-km-long fault (Fig. 2) show the MSCR for three different viscosities (Model 1a: 10^{18} Pa·s, Model 1b: 10^{19} Pa·s, and Model 1c: 10^{21} Pa·s). The difference between the results ($\sim$ 0.2 mm/year) is smaller than measurement sensitivity with the system driven by specified displacement rate along the side boundaries, and in the absence of a feature to localize strain (e.g. a fault or a shear zone), we are essentially imposing a uniform shear strain across the model domain. For this reason, the shear strain in the homogeneous viscoelastic material is constant for the different viscosities and the driving force on the fault is constant. Consequently, although an increase in viscosity will increase both the time required to reach the steady state as well as the internal stress in the viscoelastic material, it will not affect the MSCR.

Because the MSCR is dependent on the shear strain rate applied to the base of the creeping section, when the far field velocity drives the model with a uniform viscoelasticity, creep on the fault accommodates a relatively small fraction of the deformation. By including a low viscosity zone beneath the fault, we effectively localize the shear strain in the viscoelastic layer. As the contrast of viscosity between the shear zone and the rest of the viscoelastic layer is increased, more strain is localized in the shear zone. For a contrast in viscosity of three orders of magnitude and a shear zone 20 km wide (Model 3), a geometry compatible with previous thermal/rheological models for the San Francisco Bay area (Furlong and Verdonck, 1993), almost all the deformation within the viscoelastic layer is concentrated in the shear zone and creep on the fault accommodates a higher fraction of the relative displacement. It is also interesting to note that the narrower the shear zone, the more the resultant stresses will be approximated by the deep slip model of Savage and Lisowski (1993), Bürgmann et al. (2000), and Simpson et al. (2001).

Table 3
Model geometries

Model name	Model description
Model 4a	fault locked from 4 to 12 km
Model 4b	fault locked from 4 to 8 km (fault free to creep from 0 to 4 and 7 to 12 km)
Model 4c	fault locked from 6 to 12 km
Model 4d	fault entirely free to creep from 0 to 12 km
Model 5a	fault free to creep from 0 to 12 km
Model 5b	fault free to creep from 0 to 12 km, "creepable" zone extending beyond fault from 4 to 12 km
Model 5c	fault free to creep from 0 to 12 km, "creepable" zone extending beyond fault from 6 to 12 km
Model 5d	fault free to creep from 0 to 12 km, "creepable" zone extending beyond fault from 4 to 12 km in a gradational pattern
Model 6a	fault free to creep from 0 to 12 km depth for 0–41 km in length, fault locked from 4 to 12 km for 41–82 km in length
Model 6b	fault locked from 6 to 12 km for two 15 km wide zones, with 10 km between fully "creepable" to depth

All faults are 82 km long, with a 12-km-thick elastic layer and a 58-km-thick viscoelastic layer. The viscosity is 10^{18} Pa·s in the shear zone and 10^{21} Pa·s in the viscoelastic layer.

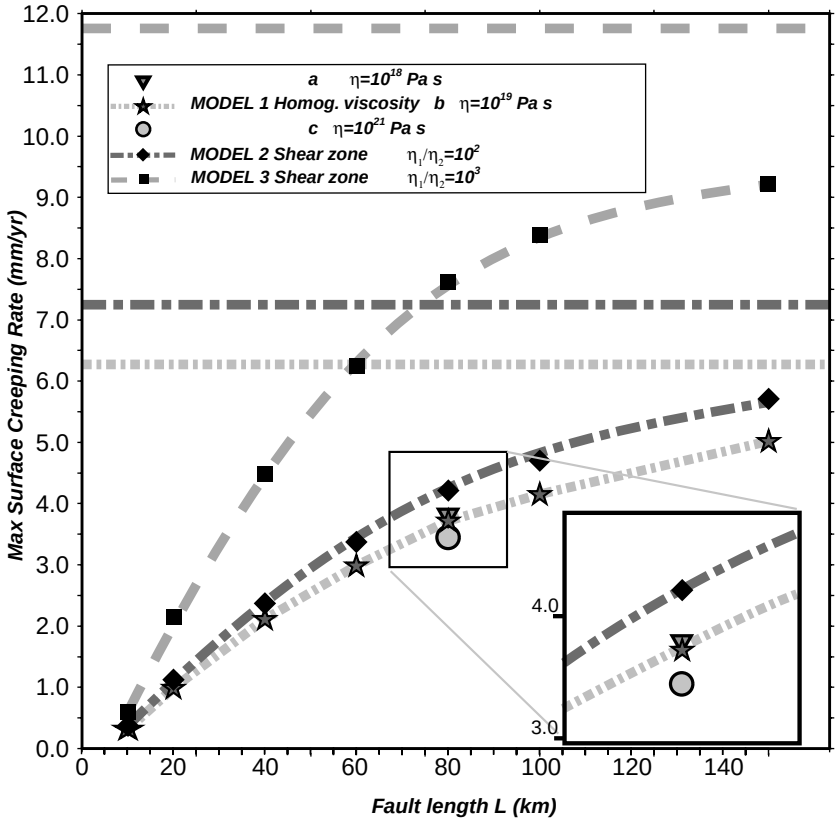

Fig. 2. Maximum creep at the surface versus fault length for different rheological models. The different symbols correspond to the results for different rheological models. The horizontal dashed lines correspond to the asymptotic value (infinite fault) for the given model while the corresponding curved lines show the interpolated exponential relationship. The three points in the insert show the results for a homogeneous model with three different viscosities.

3.3. Locking depth

Another important parameter in the analysis of the MSCR is the depth at which a "creepable" fault is no longer allowed to creep but becomes locked (Top Locking Depth, TLD). For a creeping fault in elastic half-space, Savage and Lisowski (1993) suggested that the creep rate observed at the surface on a creeping fault is related to the depth to which creep extends. This result also holds for our models although we find a somewhat different relationship between TLD and surface creep rate as compared to the relationship suggested by these previous studies, the result holds also in our model. The dashed line in Fig. 3 shows the surface creep for the Savage and Lisowski model. In general, the greater this depth, the larger the area free to creep and the faster the surface creep rate (SCR). Fig. 3 shows the MSCR for different locking depths, rheological models, and fault lengths. The pattern of creeping rate on the fault plane and the creep rate at the surface (SCR) along the fault for three different fault TLDs are plotted in Fig. 4. As expected, the MSCR increases in a nonlinear fashion as the locking depth increases for all models. In Fig. 3, we see that the infinite-length fault is more sensitive to the locking depth than a finite-length fault. In the case of a finite fault, the creep is limited by stress accumulation at the fault tips. The difference in MSCR between the different rheological and fault-length models increases as the locking depth increases. For a very shallow locking depth, where the system is dominated by the behavior of the elastic layer, the

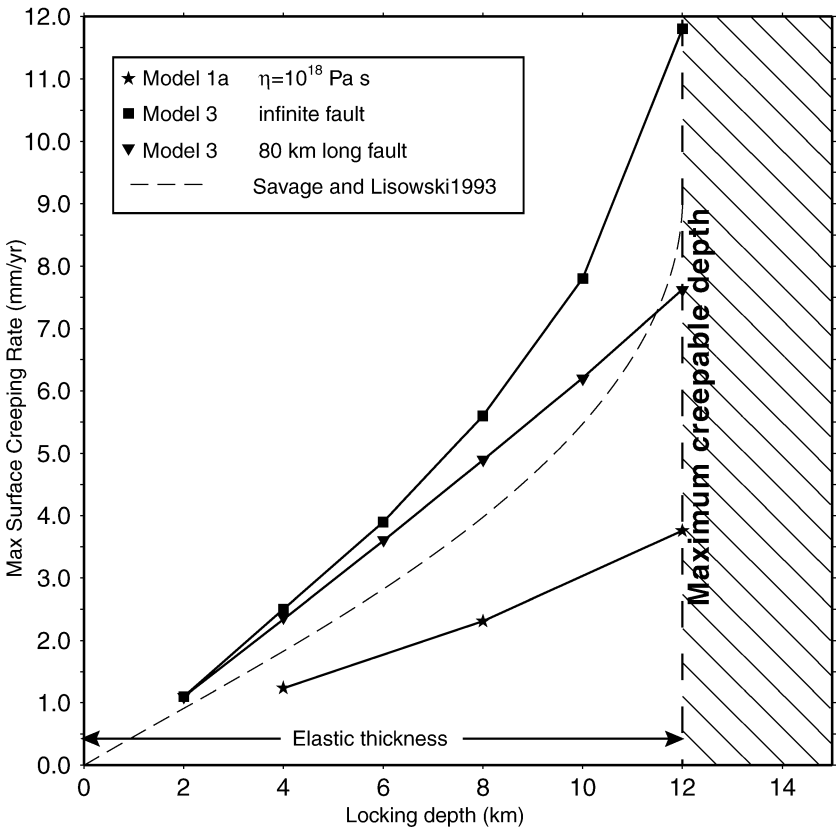

Fig. 3. Maximum creep at the surface for three different models as function of depth to the base of the creeping section (locking depth). For each model, the fault can creep from the surface down to the locking depth and is locked below this point. The maximum "creepable" depth corresponds to the elastic thickness. The inverse triangle and the square symbols correspond to a model with a low viscosity zone and different length of the "creepable" area. The star corresponds to a homogeneous viscoelastic layer. The dashed line corresponds to the result of Savage and Lisowski for an infinite fault in elastic half-space creeping to the given depth. The fault is loaded only from the dislocation beneath the seismogenic layer with a rate of 9 mm/year.

difference in MSCR is negligible. Fig. 4 compares three creeping faults of 82-km length locked to different depths and geometries. Model 4a shows the fault plane creep rate for a fault free to creep in the top 4 km and locked below this depth. Model 4b corresponds to a similar fault, free to creep down to 4 km (TLD), but locked from 4 to 8 km and "creepable" from 8 km (Bottom Locking Depth, BLD) to the bottom of the seismogenic zone. In Model 4c, the fault is free to creep from the surface to 6 km and locked below this depth. Finally, the fault is "creepable" throughout the entire seismogenic layer in Model 4d. Fig. 4e shows the surface creep rate (SCR) along the fault for the different models. As expected, when locking depth increases, MSCR increases. In the case of an 82-km-long fault with the rheology of Model 3, the MSCR increases from 2.4 mm/year for Models 4a and b (independent of the deep-creeping behavior) to 3.7 mm/year for Model 4c to 7.8 mm/year for Model 4d.

Although the "creepable" surface in Model 4b is twice as large as in Model 4a, the surface creeping patterns of the two models are indistinguishable. Furthermore, the MSCR for these two models is much smaller than that observed for Model 4c, containing a "creepable" surface intermediate area between Models 4a and b. These results suggest that the surface creep pattern is mainly influenced by the locking

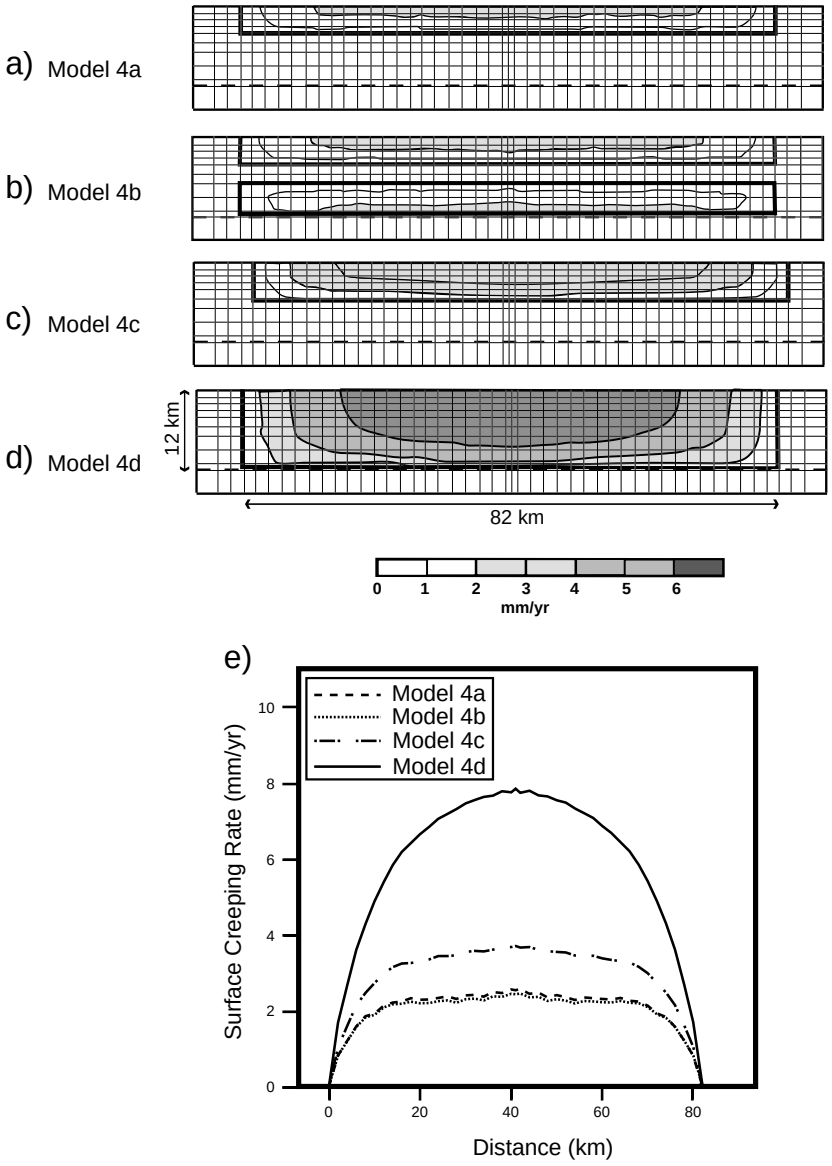

Fig. 4. (a–d) Models 4a–d contain an 82-km fault with "creepable" patches extending to various depths. "Creepable" regions are enclosed by heavy dark lines. Regions shallower than 12 km and outside "creepable" zones are locked. Regions deeper than 12 km deform in a viscoelastic way. Shading indicates creep rates on fault plane. (e) Surface creeping rate as a function of position along fault for Models 4a–d. Increasing the depth of the "creepable" zone increases the surface creeping rate. The deformation is driven by far field velocity of 30 mm/year.

depth of the creeping area connected to the surface (TLD), and is not influenced to any large extent by fault behavior beneath a locked patch. This may be an important factor to consider in seismic risk assessment. Although the surface creep patterns for Models 4a and b are the same, Model 4a has significantly larger integrated slip deficit and thus could likely generate a greater seismic moment during an earthquake (assuming 9 mm/year as the long-term slip on the 82-km fault, the seismic moment accumulated in 100 years by Model 4a would be 2.52×10^{19} Nm compared to 2.38×10^{19} Nm of Model 4b).

3.4. Fault tips and connectivity

How creeping fault segments terminate and the nature of strain accumulation at the tips of creeping sections is uncertain. Models 5a–d test some simple scenarios of fault tip behavior. Model 5a corresponds to a single, 82-km fault free to creep throughout the entire seismogenic layer. This is the geometry used to study the relationship between MSCR and fault length or locking depth. In Models 5b–d, the 82-km fault is connected at its ends with faults locked at the surface but allowed to creep below a fixed depth (BLD). The possible connections of the Hayward fault with the Calaveras fault in the south and the Rodgers Creek fault at the northern end may be geologic examples of this geometry. To simulate this interaction, we allowed the segment of the fault between $y = \pm 41$ km to creep from the surface down to 12 km and locked the fault plane from the surface to a fixed depth (BLD) elsewhere. Models 5b and c correspond to different values of BLD. Model 5d contains a smoother transition between the creeping and the locked part of the

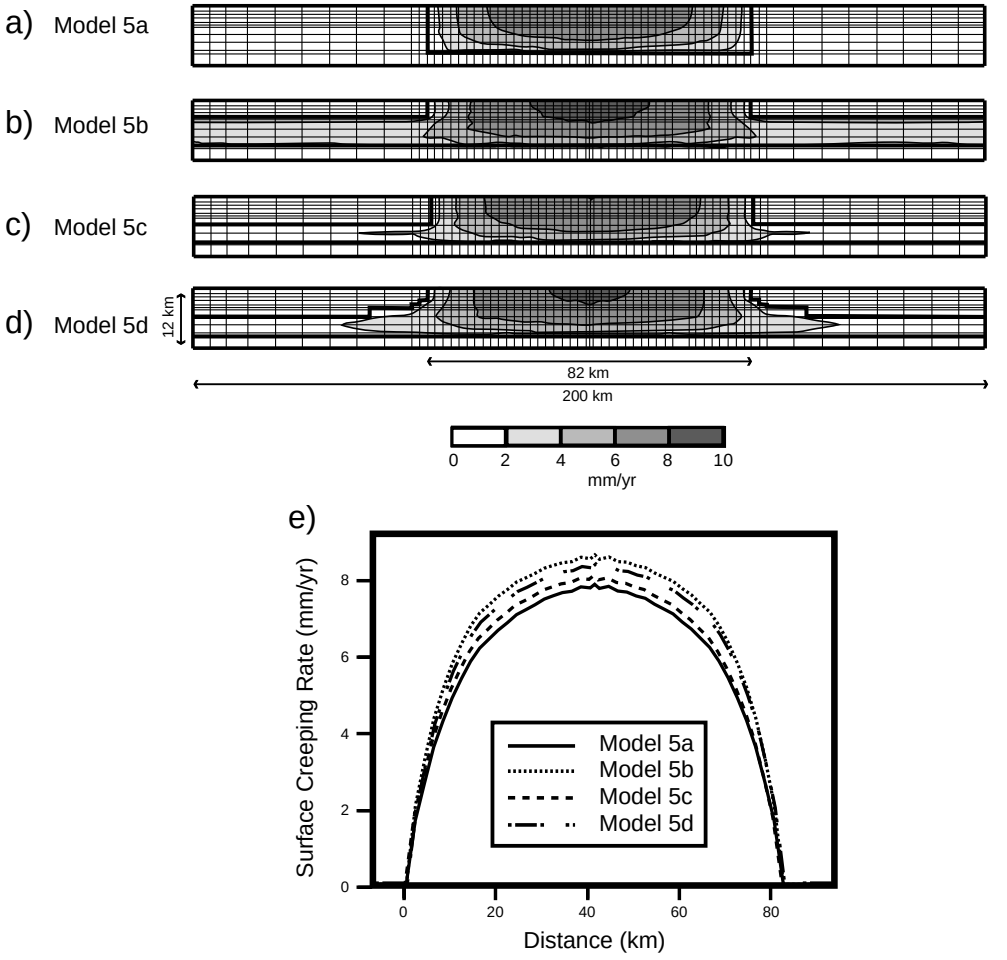

Fig. 5. (a–d) Models 5a–d contain an 82-km fault extending to the bottom of the seismogenic zone (12 km). Model 5a: Creep is only possible on the 82-km fault, extending the entire depth (12 km). For Models 5b–d, the fault is allowed to creep for the entire model length (200 km) at lower seismogenic zone depths. Model 5b: Creep extends from 4 to 12 km depth outside the fault. Model 5c: Creep extends from 7 to 12 km depth outside the fault. Model 5d: Creep zone extent outside the fault decreases from initiating at an upper depth of 4–7 km, extending to the base of the seismogenic zone at 12 km depth. (e) Surface creeping rate as a function of distance for Models 5a–d. Fault properties representation as in Fig. 4. Note that the shading scale is different from the one on the other figures.

system, with an increasing value of BLD outside the 82-km range. Despite the different creeping rates deep on the fault plane (Fig. 5a–d), the surface creep rates seen in Fig. 5e do not show significant differences and do not allow one to distinguish among the different models.

Bilham and Bodin (1992) show that the connectivity of different fault segments influences the amount of fault slip. Furthermore, with the exception of InSAR type studies, observations of creep are usually only made at discrete points along the fault. Thus, it is possible that observed creeping sections might sometimes be disconnected despite the nearness of the creeping patches. To test how isolated creeping segments influence each other, we tested a model with two separated creeping segments. We analyzed the

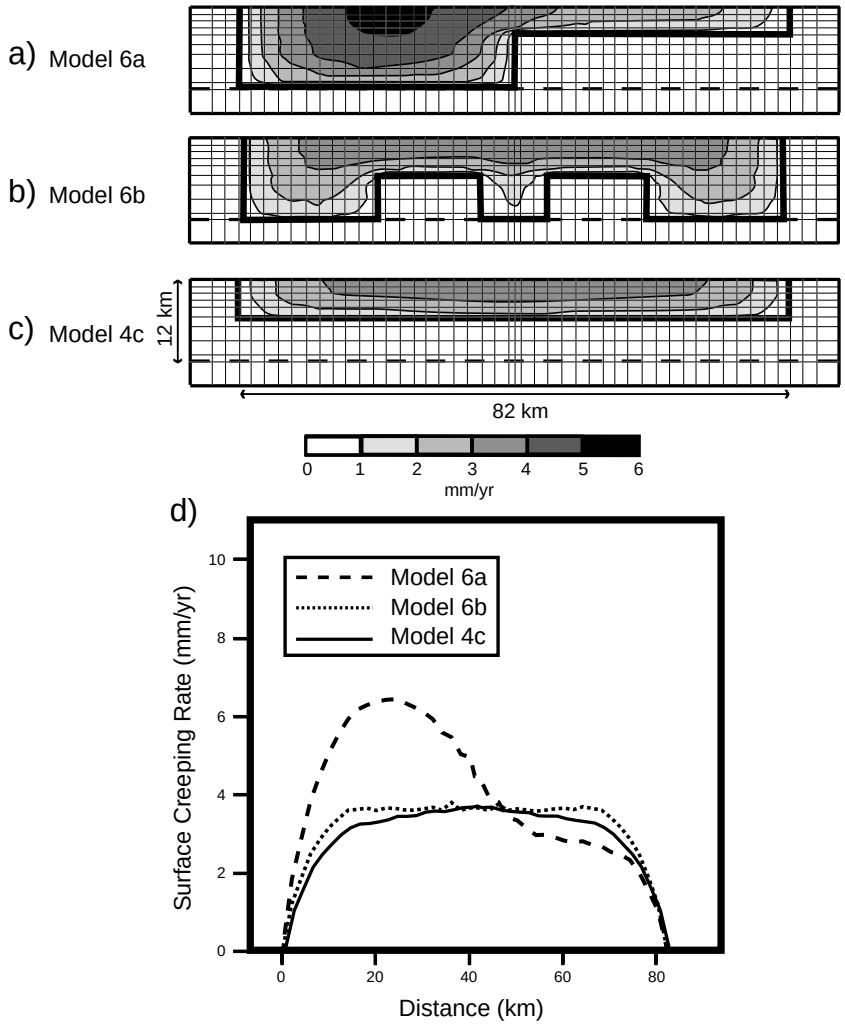

Fig. 6. (a, b) Models 6a and b contain an 82-km fault with varying patterns of locking depth. Model 6a: Creep extends from 0 to 12 km for the left half of the fault (0–41 km), and from 0 to 4 km for the right half (41–82 km). Model 6b: Two locked zones 15 km in width extend from 6 to 12 km in depth. The zones are separated in the middle of the fault with a 10-km-wide zone "creepable" to 12 km depth. (c) Model 4c is shown for comparison to demonstrate the similar behavior of Models 4c and 6b. (d) Surface creeping rate as a function of position for Models 6a, 6b, and 4c. A gradient exists in the surface creep rate from the fully creeping zone to the partially locked zone (Model 6a). Models 6b and 4c behave in a similar fashion, implying that the locked zones of Model 6b have an effect similar on surface creep to locking the entire fault from 6 to 12 km depth.

creep rate of two 40-km-long ''creepable'' faults separated by patches locked from the surface to the bottom of the seismogenic layer. For locking patches as narrow as 6 km (the shortest separation length tested), the two ''creepable'' areas behave as two independent, 40-km-long faults.

3.5. Locked patch geometry

Locked areas influence creep at the surface in a complex way. To analyze this, we tested the effects of simple-locking geometries (Fig. 6). In Model 6a, the right half of the fault is locked below 4 km and the left half is allowed to creep throughout the seismogenic zone. The surface creep rate decreased from ~ 5 mm/year over the left section to 3 mm/year in the right section. A gradient in the surface creep rate trends from the fully creeping zone to the region locked at a shallower depth. Because of this relatively smooth transition, in spite of the step discontinuity in fault zone geometry, one cannot assume that there is a one-to-one correlation between the relative magnitude of creep at the surface and the depth extent of creep on the fault at any specific location.

In Model 6b, the fault has varying locking depths of 6 and 12 km. The curve for this model is comparable with the results for a fault completely locked below 6 km (Fig. 6, Model 4c). The effect of the smooth surface creep rate transition between step discontinuities in locked/creepable areas already shown in Model 6a helps explain the lack of peaks in the SCR curve of Model 6b. The ''creepable'' section in the middle of Model 6b is too narrow to allow a significant amount of creep, further contributing to a low variability surface creep rate curve.

4. The Hayward fault

As discussed in Introduction, previous authors have modeled the observed creep along the Hayward fault in terms of patterns of creep on the fault plane reaching different interpretations in spite of reasonable similar fits to the surficial creep. Here, we apply our modeling approach to analyze the Hayward fault creeping behavior. Table 4 describes the models in this section.

Table 4
Hayward fault models

	Model description
Model 7a-B1	best-fit model from Bürgmann et al. (2000)
Model 7b-S1	model 1 from Simpson et al. (2001)
Model 7c-HN	10 km wide locked zone, (4–12 km)
Model 7d-HW	18 km wide locked zone, 4 km (7–12 km) and 14 km (4–12 km)

All faults are 82 km long, with a 12-km-thick elastic layer and a 58-km-thick viscoelastic layer. The viscosity is 10^{18} Pa·s in the shear zone and 10^{21} Pa·s in the viscoelastic layer.

The observed creep data shown in Fig. 7 are those used by Lienkaemper et al. (2001). They are comprised of decades worth of alignment arrays, offset cultural features, and creepmeters. These data are shown as points with error bars in Fig. 7, along with the model results. The observed rates show two characteristic peaks: the northern and southern ends of the Hayward fault creep faster than the middle section. Models of Bürgmann et al. (2000) and Simpson et al. (2001) have attempted to match this observed ''middle dip'' in creep rates. Likewise, in our models, we focus on the northern and middle portions of the Hayward fault, including the fall of MSCRs from the northern end to the middle of the fault. As in the previous studies, we do not attempt to model the very high rates (~ 9 mm/year) at the southern end of the Hayward fault (Lienkaemper et al., 2001; Bürgmann et al., 2000). The smooth variation of surface creep in response to changing fault behavior at depth does not allow unambiguous modeling of this behavior. The southern region of the Hayward fault and its interactions with the surrounding faults (i.e. Calaveras and Mission) increase the complexity of the system with respect to the geometry of our model. Furthermore, this part of the fault seems to be highly influenced by the Loma Prieta earthquake. While the high velocities were observed prior to the earthquake, they were significantly reduced and reversed as an effect of that event (Lienkaemper et al., 1997; Bürgmann et al., 1998).

We have first tested whether the model geometries from the previous studies produce the observed SCRs under the conditions of our model. Applying our model to the ''creepable'' fault geometries consistent with Bürgmann's model (our Model 7a-B1) and Simpson's model (our Model 7b-S1), we do not match

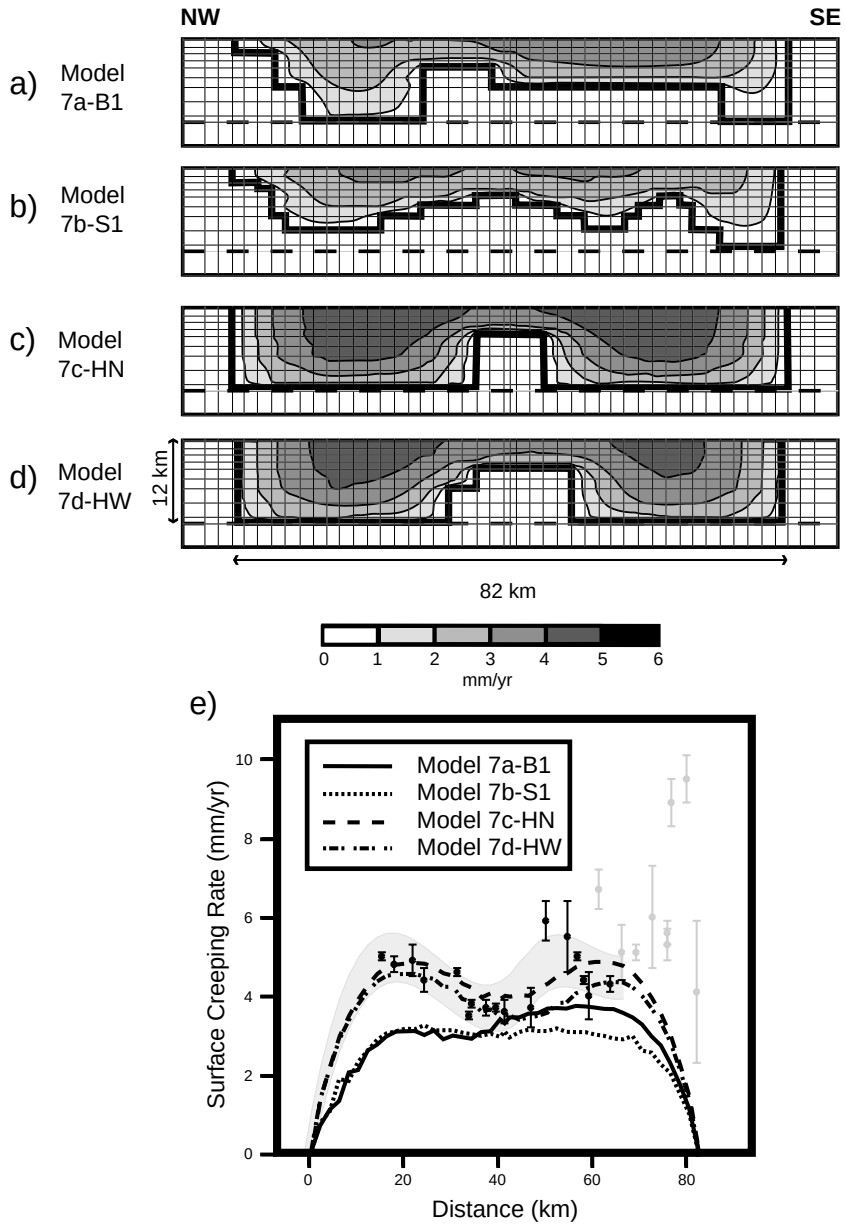

Fig. 7. Models 7a-B1 (Bürgmann et al., 2000), 7b-S1 (Simpson et al., 2001), 7c-HN (Hayward Narrow), and 7d-HW (Hayward Wide). In all models, the fault is 82 km long with varying locking depths. (a) Model 7a-B1: The distribution of "creepable" elements on the fault is varied to match the fault geometry of Bürgmann et al. (2000). (b) Model 7b-S1: "Creepable" elements on the fault are varied to fit the fault geometry of Simpson et al. (2001). (c) Model 7c-HN: A 10-km-wide locked zone extends from 4 to 12 km depth. (d) Model 7d-HW: An 18-km-wide locked zone with the geometry shown in the figure. (e) Surface creeping rate as a function of distance for Models 7a-B1, 7b-S1, 7c-HN, and 7d-HW. Models 7a-B1 and 7b-S1, based on fault geometries of previous studies, do not reproduce the pattern of the observed surface creep rates; there is a "flattening" of the curve. The models behave similarly to ones with a fixed locking zone at a depth of $\sim$ 6 km (cf. Model 4c, Fig. 4c). Models 7c-HN and 7d-HW are acceptable matches to the observed data; both reproduce the decrease in creep rate from the northern end to the middle of the fault. Data from Lienkaemper et al. (2001).

the observed creep rates (Fig. 7a–e). Surface creep patterns are significantly smoothed as compared with the geometry of "creepable" patches on the fault. That is, the SCRs do not vary significantly along the fault, and we do not generate the two peaks in the SCRs as produced by previous models. These significant differences are a result of the different rheologies and boundary conditions among the models.

Bürgmann's model focused on the differences in creep rates at the northern and middle sections, i.e. higher creep rates in the northern 20 km of the Hayward fault equates to having creep to the bottom of the seismogenic zone in their model. Our results, however, show no significant difference in SCR arising from Bürgmann et al.'s geometry. In fact, our Model 7a-B1 shows slightly higher rates at the southern two-thirds of the fault compared with the northern third, i.e. the opposite of Bürgmann's model. This apparent contradiction in creep rates is explained by the influence of fault length on creep rate results. Although the northern third of the fault extends to the viscoelastic layer, it is relatively short compared with the southern two-thirds. The longer fault length in the south allows the SCR to increase in this region (cf. Figs. 2 and 3).

Model 1 geometry from Simpson et al. (2001) (our Model 7b-S1; Fig. 7b and e) produces creep similar to our previously described Model 4c (Fig. 4c). The surface creep behaves as if the entire lower surface is locked below a depth of ~ 6 km. Varying the size and shape of the locked patches at the fine scale of Simpson et al.'s model produces only minor changes in the distribution of creep at the surface.

In our modeling, we use a far field velocity of 30 mm/year. Increasing this velocity correspondingly scales the results. Thus, it is possible to scale Models 7a-B1 and 7b-S1 to fall within the observed SCRs. However, the spatial pattern of the two peaks in the observations is still not produced; the curve retains its "flatness". One explanation for the differences among the model results may lie in the higher stresses at the bottom of the creeping fault in the Bürgmann et al. (2000) and Simpson et al. (2001) models due to the loading of the base of the fault by discrete dislocations immediately below the Hayward fault, as compared with the effects of our distributed 20-km-wide shear zone. This likely produces the smoother creep profiles in the models using our modeling approach, compared to those in prior studies.

Because the previously proposed model geometries, when analyzed with our modeling approach, do not produce the pattern in SCR observed along the Hayward fault, different geometries were tested to obtain a reasonable fit to the observations. It is possible to match observed surface creep rates using several creepable-fault geometries, two of which are shown in Fig. 7c and d. These 'best-fits' (Models 7c-HN and 7d-HW) are obtained with a relatively narrow locked portion in the center of the fault below ~ 4 km, with the two ends "creepable" to depth. These models differ with respect to Models 7a-B1 and 7b-S1, in that the locked portion of the seismogenic layer in the middle of the fault zone is relatively narrow. Because this locked zone does not extend along a significant fraction of the entire fault plane, the smoothing effect of the SCR as seen in Models 7a-B1 and 7b-S1 does not occur. The locked area has the effect of pulling down the creep rates along the middle part of the fault without decoupling the faster creeping fault segments.

5. Discussion

Determining the patterns of creep on a fault surface is an important component of assessing the potential size and rupture pattern of earthquakes along major fault strands. As shown here, different approaches to modeling the distribution of creep on the fault lead to significantly different patterns of inferred creep on the fault plane. Thus, different model approaches can imply different patterns of slip deficit to be recovered during seismic events, suggesting different results for the seismic risk analysis. In comparing our modeling results with those of the Simpson et al. (2001) and the Bürgmann et al. (2000) studies, we find some differences that are significant and need to be resolved as we improve our understanding of the Hayward fault seismic potential.

Although all the modeling approaches reasonably fit the observed data (Fig. 8), when we analyze the locked patch geometries of Simpson et al. (2001) and Bürgmann et al. (2000) with our model, we do not reproduce the pattern of creeping at the surface. Nevertheless, in comparing Simpson et al.'s (2001) results with our model 7c-HN (Fig. 9a and b), we observe that the pattern of creep on the fault plane

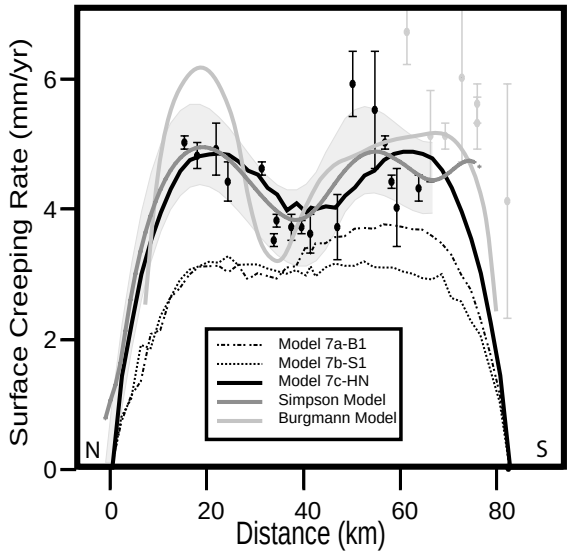

Fig. 8. Comparison between the observed geodetic data (adapted from Lienkaemper et al., 2001) and the results of our and previous models. The surface creep rate computed by our best-fit model (thick black line) fit the observed geodetic data equally well to the results of Simpson et al. (thick gray line) and Bürgmann et al. (thick light gray line). The slightly faster creep rate in the northern section in Bürgmann et al.'s model is partially due to their use of a data set with faster creep in that region which are not present in the data of Lienkaemper et al. (2001). The creeping patch geometry used by the two previous studies modeled with our approach (dashed lines) give results that do not reproduce the observed surface creeping pattern.

produced by the two models is reasonably similar. Thus, the magnitude and pattern of slip deficit on the fault inferred from both models is comparable. It is interesting to note that in these models, the accumulation of slip deficit in the northern and southern part of the Hayward fault is comparable. If correct, this has implications for earthquake hazards in the Bay area. The occurrence of the 1868 event released part of the slip deficit on the southern part of the Hayward fault; the lack of a large seismic event on the northern segment combined with the similar accumulation of slip deficit on both fault segments led to a higher risk for the northern segment with respect to the southern one.

Patterns of creep and slip deficit on the faults differ substantially between the model presented by Bürgmann et al. (2000) and our models (Fig. 9a and d). Their modeling constrained the slip below the seismogenic layer (at 12 km depth) to be at the long-term rate of 9 mm/year, localized below the fault. This produces the very high creep rates at the base of the faults as seen in Fig. 9d, and significantly changes the distribution of creep on the fault as compared with our model results. Whether such a condition of rapid localized slip is possible at the base of the seismogenic layer is not clear, but for it to exist requires a reasonably complex pattern of coupling between the elastic (seismogenic) upper crust and the lower crust and mantle beneath the fault. By including the region below the seismogenic layer in our models, we have tried to minimize this problem by allowing the system to adjust to the pattern of deformation compatible with the far field boundary conditions and the assumed rheologic model.

These differences in patterns of creep obtained by the various modeling studies point out the importance of interpreting model results in light of the model assumptions and boundary conditions. The creep pattern inferred by the models can be substantially affected by the different assumptions made in the implementation of the strain localization below the creeping fault. At present, we cannot determine the details of strain localization within the ductile layer beneath the seismogenic zone. It is possible that high resolution studies of deformation away from the creeping faults such as is possible through InSAR and similar techniques may provide some constraints on the coupling at the base of the seismogenic faults.

There are also significant differences among geometry of "creepable" patches determined in the three models. The models of Simpson et al. (2001) and Bürgmann et al. (2000) show spatially abrupt variations in fault creep, as compared with the creep pattern from the geometries that produce acceptable surface creep patterns in our modeling. This is a result of the differences in model assumptions, geometry, and boundary conditions, but also raises some interesting issues related to fault surface properties. In our models, we specify "creepable" elements—that is 'frictionless' patches that can creep if other conditions are right—with the result that in the transition between the "creepable" and locked portions of the fault, there are "creepable" regions that accumulate significant slip deficit. How these weak ('frictionless') patches will react during an earthquake is not clear. Whether they will rupture, propagate rupture, and generate seismic moment similarly to locked fault segments

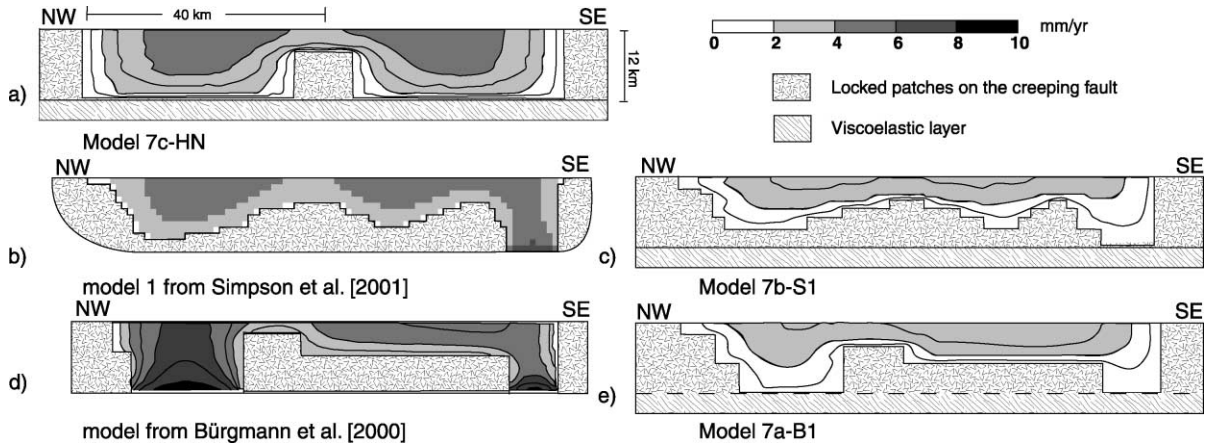

Fig. 9. Comparison of fault plane creeping patterns for different modeling approaches. (a) Model fit with the observed surficial geodetic data using approach of this paper. This figure corresponds to Fig. 7c. In order to facilitate the comparison between our models and the results from Simpson et al. and Bürgmann et al., we utilized a courser color scale than in the previous figure. (b) Best-fit model 1 result adapted from the paper of Simpson et al. (2001). (c) Creeping pattern resulting from our model for a locked geometry comparable with the one from Simpson et al.'s paper. (d) Best-fit model adapted from the paper of Bürgmann et al. (2000). (e) Results for our model utilizing the "creepable" fault geometry inferred by Bürgmann et al. The results for Simpson et al. (b) and Bürgmann et al. (d) show the creep on the upper 12 km (seismogenic layer) of the fault plane. Below this depth, the fault plane has an imposed differential slip comparable with the long-term displacement. (a), (c), and (e) show an additional layer (shaded with oblique lines) to indicate that, in our models, the fault plane ends at the base of the seismogenic layer. Beneath this depth, the region is undergoing viscous deformations. In all the models, the area shaded with edges indicates locked patches where the fault plane is not allowed to have differential displacement. The remaining area of the fault plane is allowed to creep. Note that, in our model, the transition between the locked area and the fast creeping patches is smoothed by a region with very low creeping rate not present in the Simpson et al. and Bürgmann et al. models. Note that the overall shape and amount of creep inferred by our study (gray blob in (a)) is similar to the best-fit results of Simpson et al. (b) indicating a similar slip deficit. Note the different color scale respect to the previous figures.

with similar slip deficit or if their lack of intrinsic resistance to shear will lead to different rupture character is an important question to be resolved.

6. Conclusions

The creep rate at the surface is influenced by local as well as by regional parameters. Since local parameters such as the dimension of the "creepable" area (fault length and depth of the creeping section) or the geometry of the "creepable" area influence the surface creeping behavior of a fault, it is reasonable to utilize geodetic observations to infer the creep on the fault plane. On the other hand, fault creep is also influenced by regional characteristics such as the regional stress field and the coupling with the surrounding lithosphere. Indeed, the combination of all these parameters results in a smoothing effect on the creeping behavior that does not allow one to assume a one-to-one correlation between the observed creep at the surface and the behavior on the fault plane.

In our models, the properties of the viscoelastic layer play a fundamental role in the loading characteristics of the creeping fault. For this reason, the partitioning or localization of deformation into a shear zone beneath the creeping fault significantly influences the creeping behavior of the fault.

When the results from our models are considered with respect to the Hayward fault, several conclusions can be drawn. First, the spatial resolving power of previous models (Savage and Lisowski, 1993; Bürgmann et al., 2000; Simpson et al., 2001) in defining creeping patches is not obtained with our model formulation. Further, the observed surface creep rates on the Hayward fault can be matched using several different geometries. A characteristic of all acceptable models is a narrow, locked zone near the middle of the fault. Since, based on our results and the comparison of our results with previous models, the geometry of

the creeping fault below the surface is not uniquely determined using surface creep rates, making robust estimates of seismic potential along creeping segments of faults is still problematic.

Acknowledgements

We thank Roland Bürgmann, Bob Simpson and an anonymous reviewer for the thorough reviews of the manuscript and the comments that greatly improved the paper. We are also grateful to C. Ammon, A. Nyblade, R. Engel, and C. Guzofski for the internal review of the paper and for their interesting suggestions. During the work that led to this paper, RM and KPF have been supported by the grant NSF-EAR 00-03396. We have used GMT (Wessel and Smith, 1998) to plot some of the graphs in the paper.

References

Ambraseys, N.N., 1970. Some characteristic features of the Anatolian fault zone. Tectonophysics 9, 143–165.

Argus, D.F., Gordon, R.G., 2001. Present day motion across the Coast Ranges and San Andreas fault system in central California. Geol. Soc. Amer. Bull. 113, 1580–1592.

Aytun, A., 1980. Creep measurements in the Ismetpasa region of the North Anatolian fault zone. In: Isakara, A.M., Vogel, A. (Eds.), Multidisciplinary Approach to Earthquake Prediction 2. Friedrich Vieweg & Sohn, Braunschweig/Wiesbaden. pp. 279–292.

Bilham, R., Bodin, R., 1992. Fault zone connectivity: slip rates on faults in the San Francisco Bay area, California. Science 258, 281–284.

Bürgmann, R., Fielding, E., Sukhatme, J., 1998. Geology 26, 559–562.

Bürgmann, R., Schmidt, D., Nadeau, R.M., d'Alessio, M., Fielding, E., Manaker, D., McEvilly, T.V., Murray, M.H., 2000. Earthquake potential along the northern Hayward fault, California. Science 289, 1178–1181.

DeMets, C., Gordon, R.G., Argus, D.F., Stein, S., 1994. Effect of the recent revisions to the geomagnetic reversal time scale on estimates of current plate motions. Geophys. Res. Lett. 21, 2191–2194.

Dixon, T.H., Miller, M., Farina, F., Wang, H., Johnson, D., 2000. Present-day motion of the Sierra Nevada block and some tectonic implications for the basin and range province, North America Cordillera. Tectonics 19, 1–24.

Furlong, K.P., 1993. Thermal-rheologic evolution of the upper mantle and the development of the San Andreas fault system. Tectonophysics 223, 149–164.

Furlong, K.P., Verdonck, D., 1993. Three-dimensional lithospheric kinematics in the Loma Prieta region, California: implications for the earthquake cycle. U. S. Geol. Surv. Prof. Pap. 1550-F, F103–F131.

Furlong, K.P., Hugo, W.D., Zandt, G., 1989. Geometry and evolution of the San Andreas fault zone in northern California. J. Geophys. Res. 94 (B3), 3100–3110.

Galehouse, J., 1992. Theodolite measurements of creep rates on San Francisco Bay region faults. U. S. Geol. Surv. Open-File Rep. 92–258, 256–261.

Govers, R., 1993. Dynamics of Lithospheric Extension: A Modeling Study. PhD thesis. University of Utrecht, Geologica Ultraiectina 105, 1–240.

Govers, R., Meijer, P.T., 2001. On the dynamics of the Juan de Fuca plate. Earth Planet. Sci. Lett. 189, 115–131.

Govers, R., Wortel, M.J.R., Buiter, S.J.H., 2000. Surface expression of slab break-off, results from 3D numerical models. EGS 25th General Assembly, Nice, France. Geophysical Research Abstract.

Jennings, C.W., 1994. Fault activity map of California and adjacent areas, Geologic Map number 6. Department of Conservation Division of Mines and Geology.

Lienkaemper, J., Galehouse, J., 1998. New evidence doubles the seismic potential of the Hayward fault. Seismol. Res. Lett. 69 (6), 519–523.

Lienkaemper, J., Borchart, G., Lisowski, M., 1991. Historic creep rate and potential for seismic slip along the Hayward fault, California. J. Geophys. Res. 96 (B11), 18261–18283.

Lienkaemper, J.J., Galehouse, J.S., Simpson, R.W., 1997. Creep response of the Hayward fault to stress changes caused by the Loma Prieta earthquake. Science 276, 2014–2016.

Lienkaemper, J.J., Schwartz, D.P., Kelson, K.I., Lettis, W.R., Simpson, G.D., Southon, J.R., Wanket, J.A., Williams, P.L., 1999. Timing of paleoearthquakes on the northern Hayward fault—preliminary ecidence in El Cerrito, California. U. S. Geol. Surv. Open-File Rep. 99–318, 34 pp.

Lienkaemper, J.J., Galehouse, J.S., Simpson, R.W., 2001. Long-term monitoring of creep rate along the Hayward fault and evidence for a lasting creep response to 1989 Loma Prieta earthquake. Geophys. Res. Lett. 28 (11), 2269–2272.

Lisowski, M., Savage, J.C., Prescott, W.H., 1991. The velocity field along the San Andreas fault in central and southern California. J. Geophys. Res. 96, 8369–8389.

Malservisi, R., Furlong, K.P., Dixon, T.H., 2001. Influence of the earthquake cycle and lithospheric rheology on the dynamics of the Eastern California shear zone. Geophys. Res. Lett. 28 (14), 2731–2734.

Melosh, H.J., Raefsky, A., 1980. The dynamical origin of subduction zone topography. Geophys. J. R. Astron. Soc. 60, 333–354.

Melosh, H.J., Williams, C.A., 1989. Mechanics of graben formation in crustal rocks: a finite element analysis. J. Geophys. Res. 94, 13961–13973.

Prescott, W.H., Lisowski, M., 1985. Strain accumulation along the San Andreas fault system east of San Francisco Bay, CA. Tectonophysics 97, 41–56.

Savage, J.C., Lisowski, M., 1993. Inferred depth of creep on the Hayward fault, central California. J. Geophys. Res. 98, 787–793.

Simpson, R., 2000. Watching the Hayward fault. Science 289, 1147–1148.

Simpson, R.W., Lienkaemper, J.J., Galehouse, J.S., 2001. Variations in creep rate along the Hayward fault, California, interpreted as changes in depth of creep. Geophys. Res. Lett. 28 (11), 2269–2272.

Sylvester, A.G., 1988. Strike-slip faults. Geol. Soc. Amer. Bull. 100, 1666–1703.

Toppozada, T.R., Borchart, G., 1998. Re-evaluation of the 1836 "Hayward fault" and the 1838 San Andreas fault earthquakes. Bull. Seismol. Soc. Am. 88, 140–159.

Waldhauser, F., Ellsworth, W.L., 2000. A double-difference earthquake location algorithm: method and application to the northern Hayward fault, California. Bull. Seismol. Soc. Am. 90 (6), 1353–1368.

Wessel, P., Smith, W.H.F., 1998. New improved version of generic mapping tools released. Eos Trans. - Am. Geophys. Union 79 (47), 579.